THE DISLOCATION DENSITY AND THE DISLOCATION CHARACTER EFFECT ON THE HYDROGEN PERMEABILITY OF LOW CARBON ENAMEL-GRADE STEEL

Enikő-Réka Fábián [1], Gábor Csiszár [2], Tamás Ungár [2]

[1]Budapest University of Technology and Economics, Department of Materials Science and Engineering; H- 1111, Budapest, Bertalan L. u. 7. MT building,

[2]Eötvös Loránd University, Department of Materials Physics, H-1117, Budapest, Pázmány Péter sétány 1/a., Hungary

Abstract: The role of the dislocations on the hydrogen permeation time of Al-killed, unalloyed low carbon steels was investigated using a special high resolution double crystal diffractometer operated at a rotating cobalt anode with fine focus. Strain anisotropy gives information about dislocation character and Burgers vector populations. Generally the normalized hydrogen permeation time increases or decreases with dislocation densities but the hydrogen accumulation could be less favourable near a screw dislocation than an edge dislocation.

Keywords: enamel, hydrogen, dislocation density, edge dislocation, screw dislocation

1. INTRODUCTION

For a long time there has been controversy over the extent of the effect of cold working. After Szklarska-Smialowska et al. [1] the presence of dislocations are responsible for the hydrogen diffusivity in iron at room temperature. Kumnick and Johnson [2] suggested that dislocations in iron are the source of the hydrogen trapping behaviour. Keth [3] observed that the dislocation density increased with cold work and levelled out when cold work reached 30% to 40%. Martinez-Madrid et al. [4] observed that in general the hydrogen content increased with the degree of cold work at cold worked iron, but there was a drop in the hydrogen content of specimens with 5-10% of cold work. *K. Kiuchi* and *R. B. Mc Lellan* [5] demonstrated that the dislocation density in pure iron up to 10^{13} m^{-2} has no effect on the hydrogen diffusivity. In steels the carbons modify the iron-hydrogen interaction. S Simonetti et al. [6] observed the hydrogen does not accumulate in the neighbouring of the carbon. The carbon acts such as expeller of hydrogen. The a/2 [1$\bar{1}$1] dislocation creates an energetically favourable zone for accumulation of carbon. The presences of carbon in the dislocation core make no favourable hydrogen accumulation.

Marandet [7] reported that at unalloyed carbon steels plastic deformation usually increased the total amount of hydrogen occluded. H. Huang et al. [8] at hot rolled type 1020 steel observed that hydrogen diffusivity decreased with increasing cold work and levelled out when cold work reached 30% to 40%.

The fish-scale formation on the surface of enamel coated steel products, especially if the product is enamelled on both sides, is caused by appearance and recombination of hydrogen on the sheet-enamel interface. The hydrogen can be absorbed in the metal during the enamel

firing. Hydrogen will be found not only in the normal interstitial lattice sites but also in atomic and micro-structural imperfections commonly named trapping sites [9]. Trapping enhances the solubility of hydrogen but decreases the diffusivity. The susceptibility to fish-scale formation in case of the Al-killed low carbon enamel grade steel sheets is characterized by the hydrogen permeability. That is why hydrogen permeation tests have been used for long time to estimate the hydrogen absorption capability of steel sheets used for double face enamelling. In order not to appear fish-scale on enamelled steel product surface, normalized hydrogen permeation time (T_H value) of the steel has to be: $T_H = t_0 / h^2 \geq 6.7$, where t_0 is the hydrogen permeation time [min], h is the steel sheet thickness [mm] [10-11].

P. Alexandru [12] observed at cold rolled rimmed steel for deep drawing and enamelling type A3 (STAS 9485-80) that after $\varepsilon = 20\%$ thickness reduction appeared fish-scales, and maximum number of fish-scale/m^2 appeared at 30% deformation degree.

In this work we have studied the cold rolling effect on a hot rolled and on a cold rolled and annealed unalloyed, Al- killed, low carbon steel produced for enamelling.

2. MATERIALS AND TESTING

In the experiments the cold rolling effect was studied at samples selected from hot rolled Al-killed, low carbon (LC) unalloyed strips (grade EK2) and at cold rolled and annealed samples given from DC04EK enamel-grade steel sheet. The chemical composition of the steels is given in Table 1.

Identification code/ quality	Initial state/ thickness [mm]	Chemical composition [%]								
		C	Mn	Si	P	S	Cu	Ni	Cr	Fe
MH/EK2	Hot rolled/ 2.2	0.05	0.21	0.008	0.016	0.012	0.05	0.026	0.037	rest
936/DC04EK	Cold rolled and annealed/ 0.99	0.04	0.219	0.008	0.011	0.009	0.026	0.020	0.021	rest

Table 1. *The chemical composition of the examined steels*

The materials of examined steel sheets were produced in LD steel converter, followed by continuous casting, hot rolling and pickling. The coiling temperature of Al-killed, LC enamel-grade steel is 730 ±15°C. The 936/DC04EK sheet was cold rolled in industrial condition by quarto mill. The thicknesses reduction was about 70%. The examined coil was annealed in gutter-wound coil, in bell-type annealing furnace. The annealing temperature was 670°C; with a holding time of 16 hours.

To study of cold rolling effect several sheets, approximately 40x 210 mm plates, were cut out and rolled afterwards in duo rolling mill on laboratory condition (rolls diameters were 206 mm).

The comparative deformations were calculated by:

$$\lambda_t = \frac{\sqrt{2}}{3} \sqrt{(\lambda_x - \lambda_y)^2 + (\lambda_y - \lambda_z)^2 + (\lambda_z - \lambda_x)^2} \tag{1}$$

where λ_x, λ_y, λ_z, are the true deformation in the axis x, y and z, respectively.

The hydrogen permeation time was determined by DIPERMET-H hydrogen permeability measuring equipment. Into the DIPERMET-H device two carefully degreased specimens (40x70 mm^2) were placed in a special measuring cell with sulphuric acid electrolyte above. In

6% H_2SO_4 aqueous solution 0.5 milligrams/litre As_2O_3 and 0.3 milligrams/litre $HgSO_4$ were added. The used count electrode was Pt. The current density was 125 mA/cm^2.

A semiconductor-based hydrogen detector located on the other side of the samples detects the over passing hydrogen. After each deformation level the hydrogen permeation time were measured at 4-8 specimens.

Optical microscopical examination was also carried out on longitudinal, transversal cross sections and parallel to the surface section of the sheets by a LEICA MF-4 microscope.

The microhardness measurements were carried out by Durimet microhardness tester.

For transmission electron microscopy (TEM) study the samples were polished mechanically and electrochemically. Because of the thickness of the sheets, samples were prepared only for parallel to the rolling plane condition. Examinations were carried out by JEOL JEM 200A electron microscope in half way of the dimension of the thickness.

The dislocation densities after sever deformation was determined by X-ray measurements carrying out in a special high resolution double crystal diffractometer, type Philips PW 1830, operated at a rotating cobalt anode with fine focus. The instrumental effect was negligible as compared to the physical broadening of diffraction peaks, therefore there were no need for instrumental corrections. The scattered radiation is registered by curved imaging plates of a linear spatial resolution of 50 μm. The two imaging plates were placed at a radius of 193 mm from the specimen in order to achieve the required resolution, and have covered the angular range of diffraction of about 2θ=30–170°. The samples were studied parallel with the rolling plane prepared for microscopical investigations and for EBSD study after being electro-polished.

3. SHORT SUMMARY OF THE PRINCIPLES OF EVALUATION OF THE X-RAY MEASUREMENTS

X-ray diffraction peak profile analysis is a powerful alternative to TEM for describing the microstructure of crystalline materials. X-ray diffraction peaks broaden when the crystal lattice becomes imperfect. The correlation between peak shape and specific lattice defects has been discussed in terms of the hierarchy of lattice defects by Krivoglaz [13].

Assuming that strain broadening is caused by dislocations, the full widths at half maximum (FWHM) of diffraction profiles can be given by the modified Williamson–Hall plot as [14]:

$$\Delta K \cong \frac{0,9}{D} + \left(\frac{\pi M^2 b^2}{2}\right) \cdot \rho^{1/2} K^2 \overline{C} + O(K^4 \overline{C}^2) \qquad (2)$$

where D is a size parameter characterizing the column lengths in the specimen, ρ and b are the average dislocation density and the length of the Burgers vector of dislocations. M is a constant depending on the effective outer cut-off radius of dislocations. M, can only be obtained from the tails of the profiles, therefore, it will be determined from the Fourier coefficients [15]. C, is the contrast factor of dislocations depending on the relative positions of the diffraction vector and the Burgers and line vectors of the dislocations and O stands for higher order terms in $K^4 \overline{C}^2$; $K=2\sin\theta/\lambda$ is the diffraction vector (where θ is the diffraction angle and λ is the wavelength of X-rays).

The strain fields of linear defects, especially dislocations, decay as 1/r, and are of long-range character [16]. Due to the reciprocity between crystal and reciprocal space, the scattering related to these defects decays asymptotically between ΔK^{-2} and ΔK^{-3} (where $\Delta K=(2\cos\theta_B/\lambda)\Delta\theta$, θ_B is the Bragg angle, λ is the X-ray wavelength and $\Delta\theta=\theta-\theta_B$). This scattering is clustered around the fundamental Bragg reflections and is called diffraction peak- or line broadening. Within the complex phenomena of line broadening caused by different lattice defects, dislocations play a central role. Wilkens worked out the profile shape for

dislocation arrangements and suggested to use the dislocation density (ρ) and the effective outer cut off radius (R_e) [15, 17]

The Fourier transform of line profiles given by the Warren–Averbach equation [18] is:

$$lnA(L) \cong ln\, A_L^S - 2\pi^2 L^2 g^2 <\varepsilon_{g,L}^2> , \qquad (3)$$

where A_L^S are the size Fourier coefficients, L is the Fourier parameter, and g is the diffraction vector. Strain broadening is given by the mean square strain that, in dislocated crystals is:

$$<\varepsilon_{g,L}^2> = (b/2\pi)^2 \pi\rho C f(\eta) , \qquad (4)$$

where b is the Burgers vector, ρ is the dislocation density, $f(\eta)$ is the Wilkens function, $\eta = R_e/L$, R_e is the effective outer cut off radius of dislocations and C is the dislocation contrast factor. Instead of R_e it is better to use the dislocation arrangement parameter: $M = R_e\sqrt{\rho}$ [19], which is dimension free quantity. When M is smaller or larger than unity the dipole character of dislocations is weaker or smaller, respectively. The values of C depend on the relative orientations between the line direction and Burgers vectors of dislocations and the diffraction vector and on the elastic constants of the crystal, and can be calculated numerically. In cubic crystals the dislocation contrast factors can be averaged over the permutations of the hkl indices and the following simple *hkl* dependence can be derived:

$$\overline{C} = \overline{C}_{h00}(1 - qH^2), \qquad (5)$$

where $\overline{C}_{h00}$ is the average dislocation contrast factor for the $h00$ reflections, q is a parameter depending on the elastic constants of the crystal and the edge or screw nature of the dislocations and $H^2 = (h^2k^2 + h^2l^2 + k^2l^2)/(h^2 + k^2 + l^2)^2$.

The size Fourier coefficients can be calculated for a given size distribution density function f(x). Assuming log-normal size distribution the size Fourier coefficients can be written as:

$$A^S(L) = \int_{|L|}^{\infty} \mu^2 - |L| \cdot \mu \cdot erfc \left[\frac{\log\left(\dfrac{\mu}{m}\right)}{2^{\frac{1}{2}}\sigma} \right] \cdot d\mu \qquad (6)$$

where *erfc* is the complementary error function, and m and σ are the median and the variance of the log-normal size distribution function. It can be shown that the area weighted mean coherent domain size is:

$$<x>_{area} = m\, exp(2.5\sigma^2). \qquad (7)$$

The whole profile fitting method has been worked out, in which the diffraction pattern is simulated by using ab initio physically well established functions for both, the size and the strain profile [20]. The size profile, I^S, is given by assuming either spherical or ellipsoidal crystallite shape and log-normal size distribution. For spherical crystallites, the function is defined by the two parameters: the median, m, and the variance, σ, of the size distribution function. The strain profile, I^D, is constructed by using the f(η) Wilkens function, as defined in Eq. (4). It is defined by: the dislocation density (ρ), and the dislocation arrangement parameter (M). In the simplest case, together with the q parameter in the contrast factors for cubic crystals, the numerical procedure is operating with five independent parameters: m, σ, ρ, M and q. Due to the physical nature of the microstructure, this is the minimum number of parameters which must be used. The instrumental profile, I^i, has to be measured separately.

The numerical procedure (denominated convolution multiple whole profile (CMWP) fitting procedure) is based on the convolution of the three functions, I^S, I^D and I^i :

$$I^{SIM} = I^S * I^D * I^i + I^{BG} \qquad (8)$$

where I^{BG} is the background determined before the simulated I^{SIM} function is fitted to the measured diffraction pattern.

4. RESULT AND DISCUSSION

4.1. Hot rolled low carbon Al-killed unalloyed steel

At hot rolled low carbon (LC), Al-killed unalloyed (EK2 grade) steel was observed that the *hydrogen permeability* increase exponentially as a function of the deformation degree (Fig 1.).
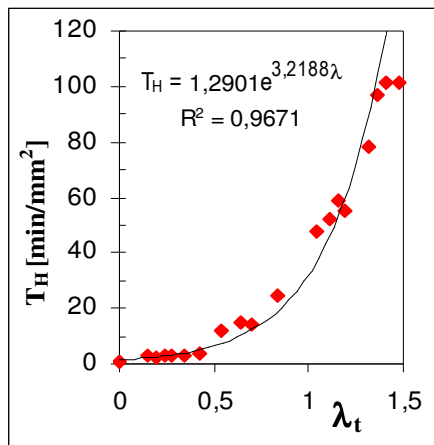

Fig. 1. *The cold rolling effect on the hydrogen permeability in case of hot rolled strip*

As one can see after some reduction level, the T_H value increased significantly. Studying them at these reduction level by optical microscope (type Leica MEF 4), each case highlights microstructural changes. The microstructure of hot rolled strip was composed from equiaxed ferrite grains (d_{gen}=26.6 μm), large carbides (some of them approximate $100\mu m^2$) and a few non metallic inclusions. Between λ_t=0– 0.347 optical microscopy did not detect significant difference in the structure of ferritic grains, however at λ_t=0.1493, at a few places cracks in the carbides revealed. Between λ_t=0.1493 and 0.4263 some broken carbides were detected. At λ_t=0.4263 value, moderate elongation of the ferrite grains was observed at samples which were prepared in longitudinal direction consistently found in previous paper [21]. After λ_t=0.537- 0.836 deformation degree, microstructure has not changed at all. Numerous carbides become fragmented, while between the carbides microcavities appear. At λ_t=0.836, each coarse-carbides was fragmented. At λ_t=1.038 the ferrite grains elongation became characteristic. With the increase of the reduction of the thickness, the extension of the ferrite grains in rolling direction became progressively more apparent.

Inhomogeneous microstructure (Fig. 2.*a),* Fig. 2 *b)*) and high dislocation densities (Fig. 2.*c)-d)*) characterized by TEM ensure us that further investigation of the dislocation structure should be carried out by alternative application. Deformation in near surface layers and in the volume of material proceeds differently also [22].
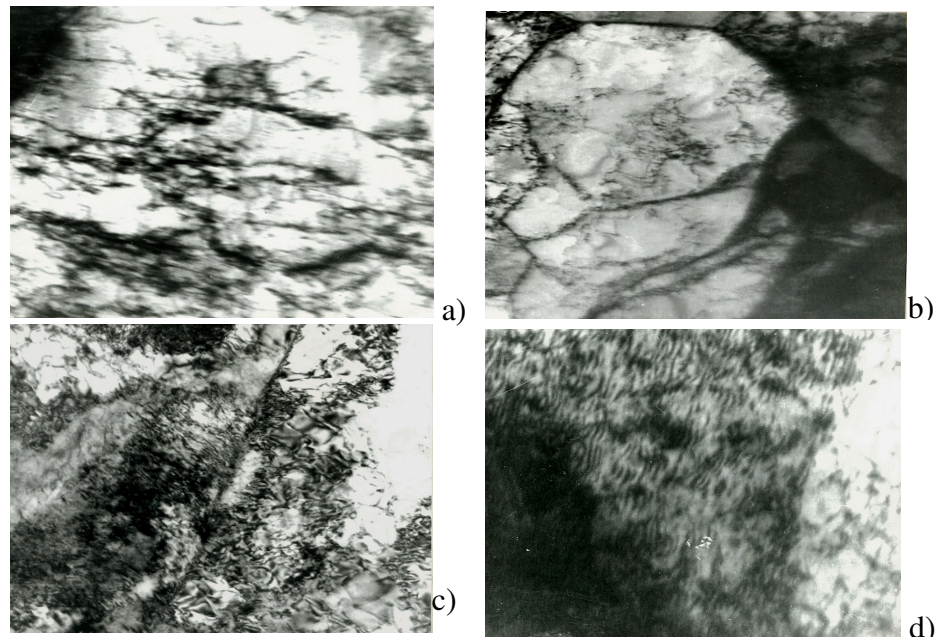

Fig. 2. *Electron micrograph of the samples from EK2-xxx series*
a) hot rolled strip; original magnification N=20 000x
b) hot rolled strip (λ_t=0); original magnification N= 30 000x
c) cold rolled λ_t=0.498; original magnification N=120 000x
d) cold rolled λ_t=0.967; original magnification N=150 000x

Therefore X-ray diffraction measurements were also carried out.

After X-ray measurements the measured diffraction profiles were fitted by theoretical calculated patterns, where the fitting provides the following 5 parameters: the median (m) and variance (σ) of the log-normal size distribution function, area weighted mean coherent domain size $<x>_a$, the average dislocation density (ρ) and the dislocation character (q). The results for samples cold rolled after hot rolling (the EK2 steel) are listed in Table 2. The hot rolled state of steel EK2 was characterized by edge dislocations ($q=1.3$), and after $\lambda_t=0.42$ deformation degree, by cold rolling, the microstructure was characterized by screw dislocations ($q=2.7$)

Samples notification	T_H value [min/mm^2]	Comparative total deformation λ_t	m [nm]	σ	$<x>_a$ [nm]	ρ [m^{-2}]	q
MH2.20	0.6	0	58	0.24	67	2.2×10^{12}	1.3_{fix}
MH1.53	4.04	0.42	36	0.33	47	3×10^{14}	2.75_{fix}
MH1.33	14.6	0.64	44	0.37	62	3.7×10^{14}	2.31
MH1.25	14.44	0.70	34	0.44	55	3.5×10^{14}	2.07
MH1.11	24.45	0.84	45	0.37	63	4×10^{14}	1.92
MH0.94	47.9	1.04	49	0.28	60	5×10^{14}	2.27
MH0.54	101.43	1.48	26	0.5	48	3.5×10^{14}	2

Table 2. *The X-ray measurements results for some cold rolled samples of EK2 steel*

Modified Williamson-Hall plots of the specimens taken out from EK2 steel after several cold rolling degree is shown in Fig. 3. The q parameters in the contrast factors correspond to the best linear fit, and are listed in the Table 2. The q parameters obtained from the *modified* Williamson-Hall plots and the CMWP whole powder pattern fittings are in good correlation.
From the modified Williamson-Hall plots one can see that the coherent domain size and the dislocation density do not differ considerably after $\lambda_t=0.63$.
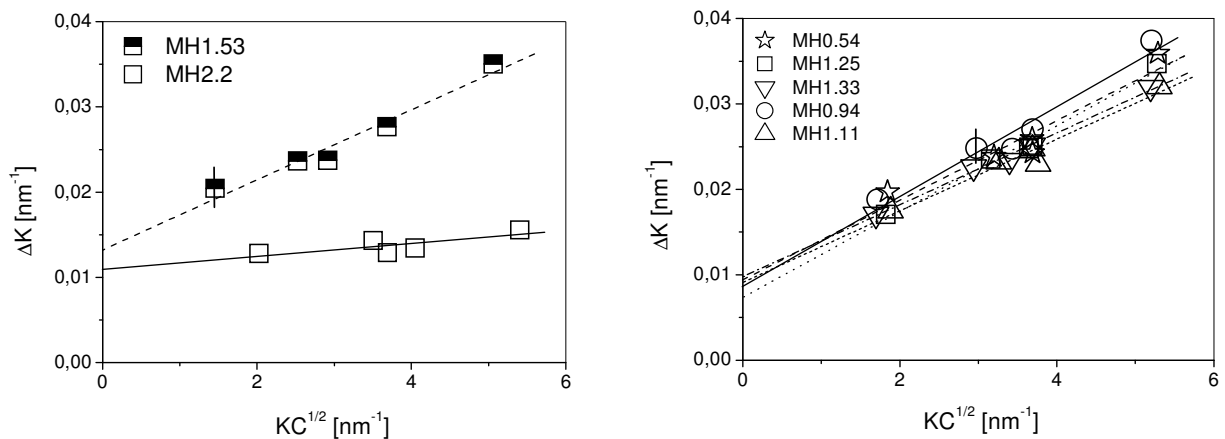

Fig. 3. *Modified Williamson-Hall plots of the specimens of EK2 steel (MH/EK2-series) corresponding to measurements in reflection geometry.*

It is noticeable that the T_H value increase with dislocation densities except for sample MH0.54 (Fig 4-5.). For sample MH1.33 ($\lambda_t=0.64$) the measured dislocation density was 3.7×10^{14}m^{-2} and the normalized hydrogen permeation time was 14.6 min, respectively. After a higher deformation degree ($\lambda_t=0.70$) the dislocation density was 3.5×10^{14}m^{-2} with a shorter T_H value (14.44 min). Despite of the value of dislocation density referring to $\lambda_t=1.48$ for samples

MH0.54, relationship between deformation level and dislocation density (Fig 4.) is consistent to previously found results in Ref. [4, 6].
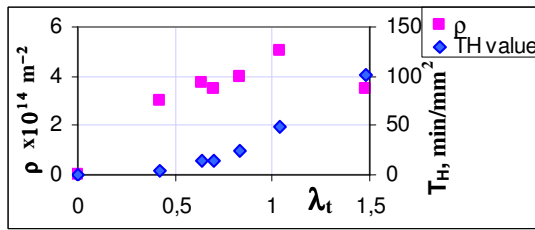

Fig.4. *Effect of true deformation on dislocation densities and on hydrogen permeability in case of the steel EK2*
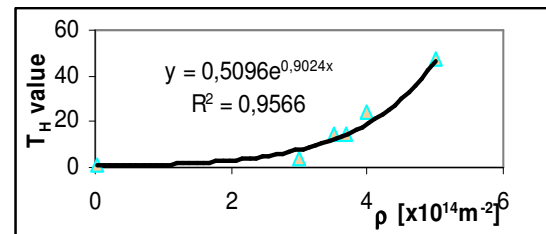

Fig. 5. *Relationship between dislocation density and hydrogen permeability of cold rolled MH/EK3 samples*

4.2. Effect of cold rolling on cold rolled and annealed enamel-grade steel.

The studied DC04EK steel was composed of equiaxed ferrite grains (98%), carbides and a few non metallic inclusions. The ferrite grain s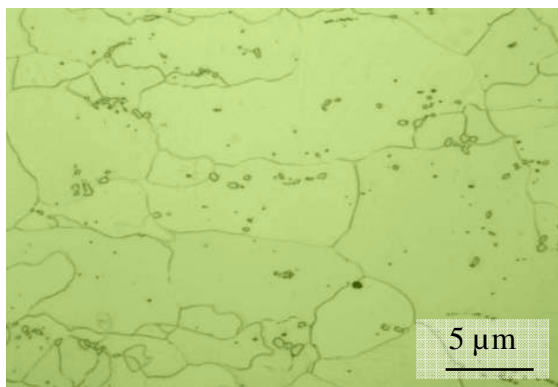ize were not uniform (Fig 6) the carbides were circular, the sizes were smaller than 3 μm^2. During the cold rolling, significant difference was not observed in microstructure. Fragmentation of the carbides was insignificant. However, the effect of cold rolling on T_H value was interesting. At these steel samples after $\lambda_t=0.34$ comparative total deformation level, the normalized hydrogen permeation time was shorter than after $\lambda_t=0.21$ deformation, while the hardness of the samples increased (Fig 7). At $\lambda_t =0.56$, a small drop was observed either in T_H value or in the micro-hardness ($HV_{0.1}$).

Fig. 6. *Micrograph of the samples DC04EK in annealed state*

The X-ray measurements results for cold rolled DC04EK samples are listed in Table 3. The annealed state with its coarse-grained feature makes impossible to determine the dislocation density by X-ray line profile analysis, however using modified Williamson-Hall plots, the magnitude of dislocation density for $\lambda_t=0$ reveals lower value by a factor of about 2 compare to that referring to $\lambda_t=0.21$. The q parameters obtained from the *modified* Williamson-Hall plots (Fig.8) and the CMWP whole powder pattern fittings are in good correlation.

Fig. 7. *The cold rolling effect on the T_H value and on the microhardness*

Samples notification	λ_t	m [nm]	σ	$<x>_a$ [nm]	ρ [m^{-2}]	q
936-000	0	-	-	-	-	-
936-085	0.21	56	0.32	72	1.3×10^{14}	1.98
936-075	0.34	32	0.43	50	1×10^{14}	2.7
936-070	0.41	42	0.34	56	2×10^{14}	1.72
936-063	0.51	33	0.5	62	3×10^{14}	2.05
936-060	0.56	31	0.47	54	2.3×10^{14}	2.5
936-054	0.67	54	0.33	71	4×10^{14}	2.07

Table 3. *The X-ray measurements results for cold rolled samples taken out from DC04EK steel*
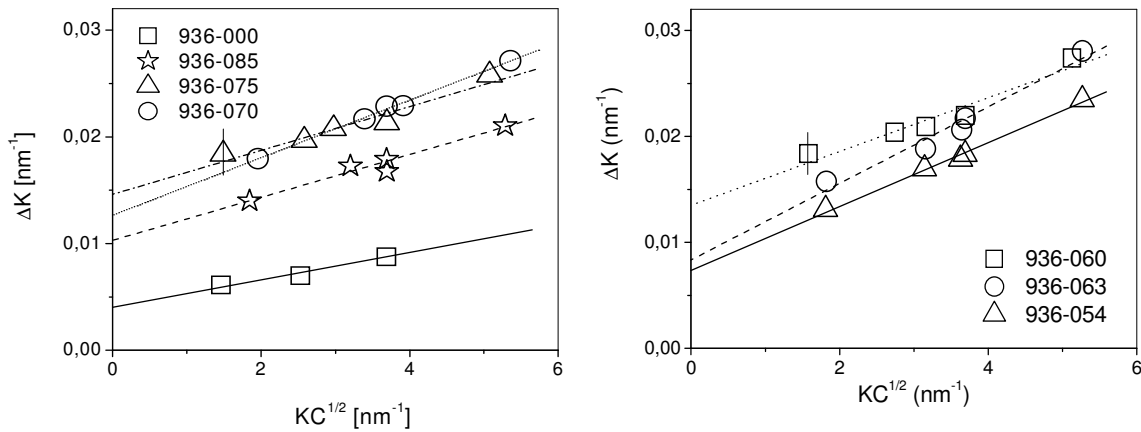

Fig. 8. *Modified Williamson-Hall plots of the specimens of 936DC04EK-series corresponding to measurements in reflection geometry*

Studying the dislocations densities and theirs character (Table 3.) one can see that the dislocations character was rather screw where T_H value reaches a minimum (λ_t=0.34). At every other samples the dislocation character was mixed. This observation is in concordance with the literature. Recently, A Juan et al. [23], studying the bonding of H-Fe by atom superposition and electron delocalization orbital cluster method, observed that when H is in the bulk iron the region near screw dislocation core is much more repulsive than in a normal Fe lattice. They considered that H accumulation could be less favorable near a screw dislocation than near an edge dislocation.

As it can be seen in Fig. 9. the T_H value increases or decreases with dislocation density, but there are not monotony. In Fig. 9. one can see that at λ_t=0.21, the average of the normalized hydrogen permeation times was 12.7 min/mm^2 and at λ_t=0.34 was less than half of it (T_H=6.275 min/mm^2) therefore the phenomenon of mixed-type and screw-type character, respectively have to be taken in consideration.
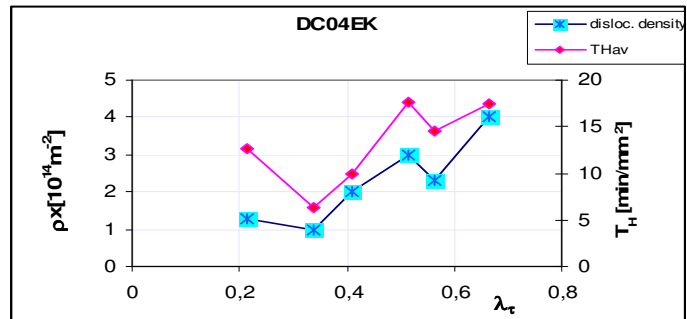

Fig. 9. *The effect of cold deformation on dislocation densities and on hydrogen permeability in case of the DC04EK steel*

5. Conclusion

X-ray line profile analysis has been well proven in studying the dislocation density and arrangement of dislocations in deformed metals. In case of non deformed hot rolled sheets characteristic dislocations is rather edge-type ($q=1.3$), and at about $\lambda_t=0.40$ it became the screw-type ($q=2.7$). In case of DC04EK specimens at $\lambda_t=0.34$ only screw dislocations were observed. At higher deformations degree, there is just as much edge-type as screw-type dislocations found in the material. Generally the T_H value increases or decreases with dislocation density, however hydrogen accumulation could be less favourable near a screw dislocation than an edge dislocation.

6. References

[1] Z. Szklarska-Smialowska and Z. Xia: *Corrosion Science,* Vol. 39, 1997, p 2171

[2] A. J. Kumnick and H. H. Johnson: Acta Met. Vol 28, 1980 p 33

[3]. A.S. Keh: "Dislocation Arrangement in Alpha Iron During Deformation and Recovery" in Direct Observation of Imperfection in Crystal, New York, Interscience Publishers, 1962), p. 213.

[4] M. Martinez-Madrid, S.L. I Chan, J.A. Charles: Hydrogen occulsivity and embrittlement in iron- effect of grain structure and cold work" Mat. Sci. and Tech., Vl, p.456 /1985

[5] K. Kiuchi , R. B Mc Lellan: Perspectives in Hydrogen in Metals, ed. by M. F. Ashby and J.P. Hirth Pergamon Press; 1990, 49

[6] S Simonetti, M. E. Pronsato, G. Brizuela and A. Juan: The electronic effect of carbon and hydrogen in an ($1\bar{1}1$) edge dislocation core system in bcc iron; Applied Surface Science, 217 (2003) p 62

[7] B. Marandet: Stress Corrosion Cracking and Hydrogen Embrittlement of Iron Base Alloys (ed. R.W. Staehle et al) National Association of Corrosion Engineers, Houston, 1977, p 775-787

[8] H. Huang and W.J.D. Shaw *Corrosion Science*, Vol. 51, 1995, No. 1, p32

[9.] Pressouyre, G. M., Bernstein I. M. Met . Trans. 1981A 12A(5): 835–844.

[10] http://www.arcelormittal.com/fce/repository/Brochures/Enamelledsteel_brochure_FR.pdf

[11] Industrial Standard MSzEN 10209

[12] P. Alexandru Metalurgia (57) 2005; 3 p 16

[13] Krivoglaz MA. Theory of X-ray and thermal neutron scattering by real crystals. Berlin: Springer-Verlag; 1996.

[14] T. Ungár, A. Borbély, Appl. Phys. Lett. 69 (1996) 3173

[15] Wilkens M. Phys Stat Sol (a) 1970;2:359.

[16] T. Ungar: Microstructural parameters from X-ray diffraction peak broadening Scripta Materialia 51 (2004) 778

[17] Wilkens M. In: Simmons JA, de Wit R, Bullough R, editors. Fundamental aspects of dislocation theory. Vol. II. Nat Bur Stand (US) Spec Publ No 317, Washington, DC, USA, 1970. p. 1195.

[18] Warren BE. Progr. Metal. Phys. 1959;8:147.

[19] Groma I. Phys RevB 1998;57:7535.

[20] Ribarik G, Ungar T, Gubicza J. J Appl. Cryst. 2001; 34:669.

[21] Enikő-Réka Fábián, László Dévényi; Materials Science Forum Vol. 537-538 (2007) p. *33-40*

[22] A.Ciupliys, j. Vilys, C Ciuplis, V Kvedaras: Investigation of dislocation structure of low carbon steel during static loading; ISSN 1392-1207. Mechanica,2006 Nr4(60) :64

[23] A. Juan, B. Irigoyen, S. Gesari: Applied Surface Science 172 (2001) p. 11–12